

Coexisting and multiple scroll attractors in a Hopfield neural network with a controlled memristor

Qing-Qing Ma(马青青), An-Jiang Lu(陆安江), and Zhi Huang(黄智)

Citation: Chin. Phys. B, 2024, 33 (**12**): 120502. DOI: 10.1088/1674-1056/ad8148
Journal homepage: http://cpb.iphy.ac.cn; http://iopscience.iop.org/cpb

What follows is a list of articles you may be interested in

Fractional-order heterogeneous memristive Rulkov neuronal network and its medical image watermarking application

Dawei Ding(丁大为), Yan Niu(牛炎), Hongwei Zhang(张红伟), Zongli Yang(杨宗立), Jin Wang(王金), Wei Wang(王威), and Mouyuan Wang(王谋媛)
Chin. Phys. B, 2024, 33 (**5**): 050503. DOI: 10.1088/1674-1056/ad322b

Coexistence behavior of asymmetric attractors in hyperbolic-type memristive Hopfield neural network and its application in image encryption

Xiaoxia Li(李晓霞), Qianqian He(何倩倩), Tianyi Yu(余天意),Zhuang Cai(才壮), and Guizhi Xu(徐桂芝)
Chin. Phys. B, 2024, 33 (**3**): 030505. DOI: 10.1088/1674-1056/acf281

FPGA implementation and image encryption application of a new PRNG based on a memristive Hopfield neural network with a special activation gradient

Fei Yu(余飞), Zinan Zhang(张梓楠), Hui Shen(沈辉), Yuanyuan Huang(黄园媛), Shuo Cai(蔡烁), and Sichun Du(杜四春)
Chin. Phys. B, 2022, 31 (**2**): 020505. DOI: 10.1088/1674-1056/ac3cb2

Controlling chaos and supressing chimeras in a fractional-order discrete phase-locked loop using impulse control

Karthikeyan Rajagopal, Anitha Karthikeyan, and Balamurali Ramakrishnan
Chin. Phys. B, 2021, 30 (**12**): 120512. DOI: 10.1088/1674-1056/ac1b83

New results for exponential synchronization of linearly coupled ordinary differential systems

Ping Tong(童评), Shi-Hua Chen(陈士华)
Chin. Phys. B, 2017, 26 (**5**): 050503. DOI: 10.1088/1674-1056/26/5/050503

Coexisting and multiple scroll attractors in a Hopfield neural network with a controlled memristor

Qing-Qing Ma(马青青), An-Jiang Lu(陆安江)†, and Zhi Huang(黄智)

College of Big Data and Information Engineering, Guizhou University, Guiyang 550025, *China*

(Received 13 August 2024; revised manuscript received 24 September 2024; accepted manuscript online 30 September 2024)

A method of generating multi-double scroll attractors is proposed based on the memristor Hopfield neural network (HNN) under pulse control. First, the original hyperbolic-type memristor is added to the neural network mathematical model, and the influence of this memristor on the dynamic behavior of the new HNN is analyzed. The numerical results show that after adding the memristor, the abundant dynamic behaviors such as chaos coexistence, period coexistence and chaos period coexistence can be observed when the initial value of the system is changed. Then the logic pulse is added to the external memristor. It is found that the equilibrium point of the HNN can multiply and generate multi-double scroll attractors after the pulse stimulation. When the number of logical pulses is changed, the number of multi-double scroll attractors will also change, so that the pulse can control the generation of multi-double scroll attractors. Finally, the HNN circuit under pulsed stimulation was realized by circuit simulation, and the results verified the correctness of the numerical results.

Keywords: multi-double scroll attractors, Hopfield neural network, pulse control

PACS: 05.45.–a **DOI:** 10.1088/1674-1056/ad8148

1. Introduction

In nature, the brain is a neural network of countless biological neurons that interact through synapses, transmit biological information, and control the basic activities of biological organisms.[1,2] It has been found that a number of neurological disorders are associated with the activity of neurons in the neural network, and in order to further understand the chaotic behavior exhibited by neurons, researchers designed artificial neural network, which usually consists of single or multiple artificial neurons.[3–7] Among the existing artificial neural network models, the Hopfield neural network is usually used to simulate the structure and behavior of the brain because of its unique lattice structure and diverse topological types, as well as its strong nonlinear characteristics, rich chaotic dynamics and easy hardware implementation.[8–12]

As the fourth basic component in the circuit, the memristor is non-volatile, which is similar to the synaptic plasticity in the neural network.[13] In the neural network, replacing the original synaptic weight with the memristor synaptic weight can show more interesting dynamic behaviors. In the study of memristive HNN, the synapses in the neural network are replaced by different types of memristors. Bao B, Qian H and Xu Q[14] designed a new hyperbolic-type memristor and replaced the synaptic weight with a memristor synaptic weight, discovered the asymmetric attractor coexistence, and proved that the proposed hyperbolic memristor has a stabilization effect on chaotic HNN. Lai Q and Chen Z[15] added a flux-controlled non-volatile memristor to a simple three-dimensional chaotic system so that the chaotic system has a higher dimension and the scroll attractor can be observed. Lin H, Wang C, Hong Q and Sun Y[16] established a memristive Hopfield neural network by utilizing the multi-stable memristor as a memristor synapse. The memristive neural network generates infinitely many coexisting chaotic attractors that enjoy the same structure.

In addition, the dynamic behavior of neurons or neural networks can be affected by external electromagnetic radiation or the internal membrane potentials of neurons.[17–21] Appropriate electromagnetic radiation promotes intermittent synchronization of neurons, but excessive electromagnetic radiation can lead to neurological disorders and cause abnormal neuronal discharges, which can induce neurological disorders like Psychosis[22] and Alzheimer,[23] whereas appropriate stimulation with electromagnetic radiation can positively affect organisms and modify the chaotic dynamics of the nervous system. Therefore, the use of electromagnetic radiation to induce more complex dynamical behaviors is gradually gaining attention. Through comparative experiments, Lin H, Wang C, Yao W and Tan Y[24] found that applying electromagnetic radiation to a single neuron in a neural network topology can induce a large number of chaotic attractors, while multi-scroll attractors can also be generated when electromagnetic radiation and multi-level pulse stimulation are applied simultaneously. Zhang S, Zheng J H and Wang X[25] proposed a new nonequilibrium Hindmarsh–Rose (HR) neuron model with memristive electromagnetic radiation effects, which is unique in that hidden attractors with complex topologies can be generated and the parity of the scroll can be conveniently

†Corresponding author. E-mail: ajlu@gzu.edu.cn

© 2024 Chinese Physical Society and IOP Publishing Ltd

controlled by changing the internal parameters of the memristor.

By reviewing the existing memristor HNN, an obvious problem can be found, the researchers pay more attention to the effect of replacing synapses with memristor on the dynamical behavior of neural network, and the main purpose is to construct memristor systems with chaotic behaviors such as chaos, hyperchaos, coexisting attractors, and hidden attractors.[26–30] However, it is an important challenge to effectively control and regulate chaotic behavior in memristor neural networks. How to control the number of multiple vortex attractors by pulse stimulation of memristors so as to precisely regulate the dynamic behavior of chaotic systems and apply it to the optimization and reinforcement learning of neural networks, there is still a large research gap. Compared with the conventional double scroll attractors, the multi-scroll attractors have a more complex topology and can generate more key parameters with higher pseudo-randomness, which provides higher security in chaotic engineering applications, such as in the field of digital signal encryption.[31,32]

The higher randomness and unpredictability are also consistent with the complex chaotic dynamical behavior in biological neural networks, which is important for understanding some physiological processes in living beings and the cure mechanism of neurological diseases.

In this paper, two different cases of chaotic dynamics of neural network are investigated. Firstly, adding original hyperbolic-type memristor to the HNN so that the effect of memristor synapses on the dynamic behavior of the HNN can be described. Then, adding a multi-level-logic signal pulse to the memristor, the change of the HNN dynamic behavior is discussed without changing the network topology. The numerical simulation results show that when the original memristor is added, changing the internal parameters of the memristor can lead to showing single scroll, double scroll attractors and coexistence of various asymmetric attractors in the new HNN. In addition, it was found that when the memristor is stimulated with pulses, it causes the system to generate 2, 4 and 8 sets of multiple scroll attractors, and the number of scrolls can be controlled by pulses. Stimulating the memristor with pulses to control the number of multiple scroll attractors is not common in the existing HNN chaotic system.

2. HNN with hyperbolic-type memristor

In this section, the memristor HNN is mathematically modeled and the equilibrium and stability of the system are analyzed.

2.1. Hyperbolic-type memristor HNN mathematical model

HNN is a kind of recurrent neural network, containing n neurons and each neuron is connected to each other. In this paper, we choose the common hyperbolic tangent function as the neural activation function, and the circuit equation of the i neuron can be expressed by

$$C_i \frac{\mathrm{d}x_i}{\mathrm{d}t} = -\frac{x_i}{R_i} + \sum_{j=1}^{n} w_{ij} \tanh(x_j) + I_i, \tag{1}$$

where x_i is a variable standing for the voltage across the capacitor C_i, R_i is the membrane resistance between the inside and outside of the neuron, I_i is the input bias current of the neuron, $\tanh(x_i)$ is the neuron activation function for the voltage input of the j neuron, and w_{ij} is a matrix of synaptic weights indicating the strength of the connection between the i and j neurons. This synaptic weight is represented by a resistance in the circuit. A HNN model based on a hyperbolic memristor can be easily proposed when replacing the synaptic weight resistor with a hyperbolic-type memristor. The connection topology is shown in Fig. 1.

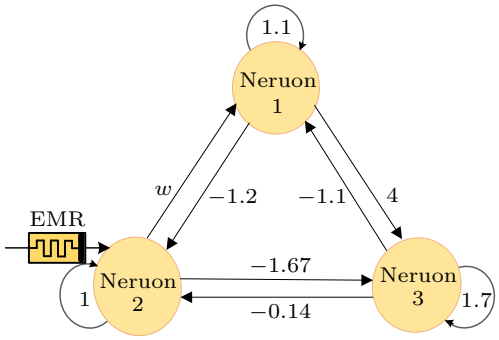


Fig. 1. Connection topology for hyperbolic-type memristor based HNN.

Memristors can be used to simulate biological synapses, and the memristor model used in this paper is as follows:

$$\begin{cases} I = W(\varphi)V, \\ W(\varphi) = a - b\tanh(\varphi), \\ \varphi' = V - \varphi, \end{cases} \tag{2}$$

where V, I and φ respectively represent the input voltage, output current and memristor function, $W(\varphi)$ is a continuous function, and a and b are the memristor parameters.

For this connection topology, the connection matrix considered has the following form:

$$W_{ij} = \begin{bmatrix} w_{11} & W(\varphi) & w_{13} \\ w_{21} & w_{22} & w_{23} \\ w_{31} & w_{32} & w_{33} \end{bmatrix} = \begin{bmatrix} 1.1 & W & 1.1 \\ -1.2 & 1 & -0.14 \\ 4 & -1.67 & 1.7 \end{bmatrix}. \tag{3}$$

In this matrix, w_{21} stands for synaptic weights between the second and first neurons. Then w_{21} was replaced by a hyperbolic-type memristor $W = a - b\tanh(w)$ with a memristor strength of 1, where $a = 3.6$, $b = 0.1$. Internal parameters

of the memristor: $c = 1.3$. Let $n = 3$, $C_i = 1$, $R_i = 1$, $I_i = 0$ and $RC = 1$. The ordinary equation with dimensionless autonomy describing the memristor HNN is

$$\begin{cases} \dot{x} = -x + 1.1\tanh(x) + W\tanh(y) + 1.1\tanh(z), \\ \dot{y} = -y - 1.2\tanh(x) + \tanh(y) - 0.14\tanh(z), \\ \dot{z} = -z + 4\tanh(x) - 1.67\tanh(y) + 1.7\tanh(z), \\ \dot{w} = -w + c\tanh(x). \end{cases} \tag{4}$$

Therefore, the HNN based on hyperbolic-type memristor can be modeled by the above equation.

2.2. Equilibrium and stability analysis

Setting the left-hand of Eq. (4) to zero, the solution of the equation is the equilibrium point of the memristor HNN

$$\begin{cases} 0 = -x + 1.1\tanh(x) + W\tanh(y) + 1.1\tanh(z), \\ 0 = -y - 1.2\tanh(x) + \tanh(y) - 0.14\tanh(z), \\ 0 = -z + 4\tanh(x) - 1.67\tanh(y) + 1.7\tanh(z), \\ 0 = -w + 1.3\tanh(x). \end{cases} \tag{5}$$

Let $h_1 = \mathrm{sech}^2(x)$, $h_2 = \mathrm{sech}^2(y)$, $h_3 = \mathrm{sech}^2(z)$, $h_4 = \mathrm{sech}^2(w)$, $k_1 = \tanh(w)$, $k_2 = \tanh(y)$, the Jacobi matrix of this system at any equilibrium point can be given by

$$J = \begin{bmatrix} 1.1h_1 - 1 & (a - bk_1)h_2 & 1.1h_3 & -bk_2h_4 \\ -1.2h_1 & h_2 - 1 & -0.14h_3 & 0 \\ 4h_1 & -1.67h_2 & 1.7h_3 - 1 & 0 \\ dh_1 & 0 & 0 & 0 \end{bmatrix}. \tag{6}$$

In Eq. (4), the right-hand side is a group of transcendental functional equations, which can be easily solved for the zero equilibrium point $E = (0,0,0,0)$. The characteristic polynomial of the equilibrium point E can be expressed as

$$\begin{aligned} P(\lambda) &= \det(1\lambda - J) \\ &= (\lambda + 1)[\lambda^3 - 0.8\lambda^2 \\ &\quad + (1.2a - 4.7038)\lambda - 0.28a - 2.181]. \end{aligned} \tag{7}$$

It can be seen through Eq. (6) that the eigenvalue of the equilibrium point E is only related to the parameter a of the memristor. Taking $a = 3.6$, the eigenvalues can be found to be respectively $\lambda_1 = -1$, $\lambda_{2,3} = -0.5283 \pm 1.1994\mathrm{i}$, and $\lambda_4 = 1.8565$. So the equilibrium point E_0 is the unstable indicator 1 saddle focus. For nonzero equilibrium points $E_2 = (m_1, m_2, m_3, m_4)$ and $E_2 = (n_1, n_2, n_3, n_4)$, their equilibrium points require graphical analysis to be solved. Therefore, Eq. (4) is rewritten as following equations containing the analytic formulas of $f_1(x,z)$ and $f_2(x,z)$ curves:

$$\begin{aligned} w &= 1.3\tanh(x), \\ y &= a\tanh\left(\frac{-z + 4\tanh(x) + 1.7\tanh(z)}{1.67}\right), \\ f_1(x,z) &= -x + 1.1\tanh(x) + (a - b\tanh(w))\tanh(y) \\ &\quad + 1.1\tanh(z), \end{aligned}$$

$$f_2(x,z) = -y - 1.2\tanh(x) + \tanh(y) - 0.14\tanh(z). \tag{8}$$

In Fig. 2, the green solid line indicates the $f_1(x,z)$ curve, the green dashed line indicates the $f_2(x,z)$ curve, and the intersection of the curves is the position of the equilibrium point.

By graphical analysis, the equilibrium point E_1 is found to be $E_1 = (-0.1021, -0.2870, 1.6352, -0.1323)$ and E_2 is found to be $E_2 = (0.1020, 0.2895, -1.6406, 0.1321)$. By substituting the equilibrium point E_1 into the Jacobi matrix (6), the characteristic root corresponding to this equilibrium point can be found to be $\lambda_{1,2} = 0.0611 \pm 1.8345\mathrm{i}$, $\lambda_3 = -0.8611$, $\lambda_4 = -1.0108$, so E_1 is an indicator of instability 2 saddle focus. Similarly, the characteristic root of the equilibrium point E_2 can be found to be $\lambda_{1,2} = 0.0523 \pm 1.8414\mathrm{i}$, $\lambda_3 = -0.8693$, $\lambda_4 = -0.9886$ so E_2 is also an indicator of instability 2 saddle focus.[33]

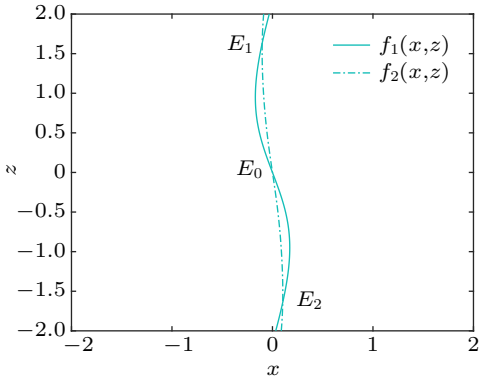


Fig. 2. Two function curves and their intersection points, where $a = 3.6$ and $b = 0.1$.

3. Dynamic analysis and numerical simulation

3.1. Analysis of dynamic behavior with parameter *a*

In order to analyze the influence of a hyperbolic-type memristor on HNN, parameter a of the memristor is set as the bifurcation parameter, and its bifurcation diagram and Lyapunov exponent spectrum are discussed. Fixing the parameters of the network unchanged, setting parameter $b = 0.1$, $c = 1.3$, besides the initial value conditions are set to (1, 1, 1, 1). When parameter a varies between [3, 5], the Lyapunov exponential spectrum and bifurcation diagram of HNN are shown in Fig. 3.

It can be seen from the bifurcation diagram and Lyapunov exponential spectrum that the dynamic behavior of this HNN changes gradually with the increase of parameter a. When $a \in [3.1, 3.25]$, the system enters chaos by period-doubling bifurcation. When $a \in (3.25, 4.17]$, chaotic traces appear in both the upper and lower half regions of the bifurcation diagram. In this case, chaotic attractors with two scrolls can be observed in the x–y plane. With the increasing of parameter a, when $a \in (4.17, 4.30]$, the plot trace of the upper half of the bifurcation diagram disappears, and only the single scroll attractor with downward scroll direction can be observed in the phase

diagram of the x–y plane. When $a \in [4.3, 4.62]$, the downward direction of the single scroll attractor disappears. Especially, it can be observed from the phase diagram that after period window ($a \in [4.42, 4.54]$), the upward single scroll attractor appears again from chaos to period to chaos. This also indicates that the system switches quickly between periodic and chaotic states. When $a \in [4.62, 4.89]$ and $a \in (4.89, 5]$, respectively, the periodic and quasi-periodic states of the different scroll attractors can be observed in the phase diagram, and finally the HNN stabilizes in the periodic state. The phase diagram in Fig. 4 is consistent with the bifurcation diagram and the Lyapunov exponential spectrum analysis. Note that Wolf's method was used to calculate the finite-time Lyapunov exponents, where the MATLAB ODE45 algorithm with time-step 0.1 s and time-end 10 ks is utilized.

To further analyze the effect of parameter a on the dynamic behavior of HNN, Fig. 4 shows the phase diagram of different parameters a in the x–y plane. In Fig. 4(a), the periodic state at $a = 3.18$ and the double scroll attractors at $a = 3.6$ can be observed. In Fig. 4(b), a single scroll attractor with different scroll directions can be observed when $a = 4.18$ and $a = 4.35$. In Fig. 4(c), the periodic state, the periodic single scroll attractor and the quasi-periodic attractor can be observed when $a = 4.45$, $a = 4.55$, $a = 4.65$, respectively.

These results of the phase diagram are consistent with the bifurcation diagram and Lyapunov exponential spectrum analysis. The above analyses can more accurately simulate the function of the HNN, in the meantime, they also demonstrate that when the synaptic resistor in the original HNN is replaced with a hyperbolic-type memristor, more abundance will be observed.

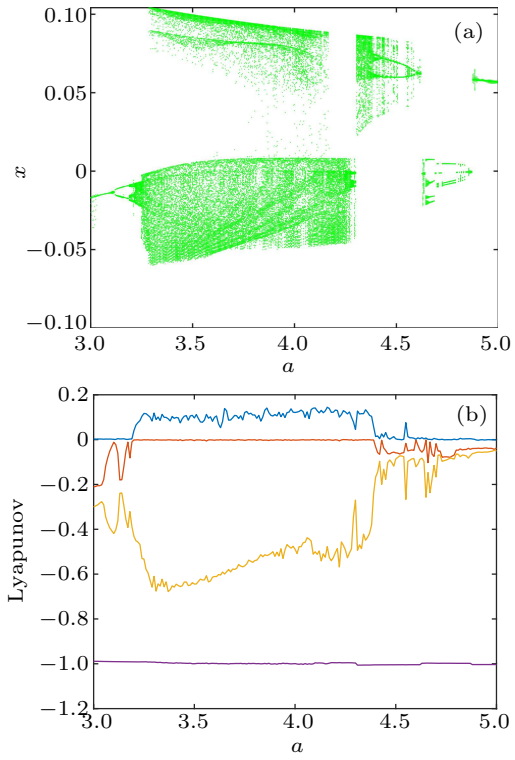


Fig. 3. The dynamic behavior of the HNN model (3) when parameter a changes: (a) the bifurcation diagram, (b) the Lyapunov exponent spectrum.

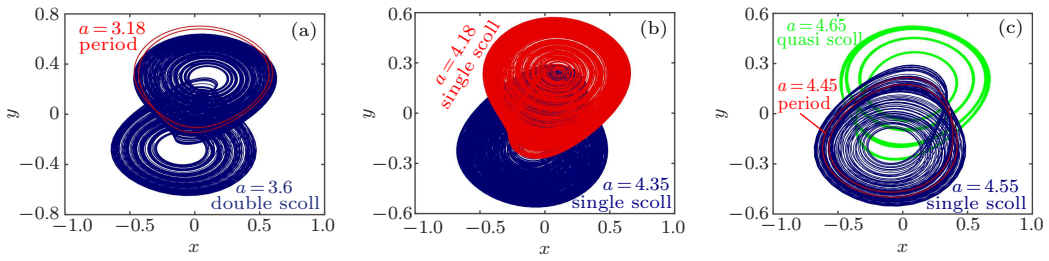


Fig. 4. Different types of attractors with different values of a.

3.2. Attractor coexistence analysis

In order to analyze the dynamic behavior of this system more deeply, the parameter a of the hyperbolic-type memristor is selected as the bifurcation variable. The coexistence of period, chaos and scroll attractor in this HNN system can be observed by setting different initial conditions of state variables. Firstly, system parameters b and c are set to $b = 0.1$, $c = 1.3$. Then Fig. 5 shows the bifurcation with different values of a from 4 to 5, where initial value conditions (x, y, z, w) are set to $(1,1,1,1)$, $(1,-1,1,1)$, and $(-0.1,-0.1,0,0)$ and correspond to the green line, blue line and red line respectively in Fig. 5.

The coexistence of various attractors can be seen in Fig. 6. As shown in Fig. 6(a), when $a = 4.24$, the coexistence of a double scroll attractor and a single scroll attractor can be observed in the phase diagram. In order to observe the coexistence phenomenon explicitly, the single scroll attractor is

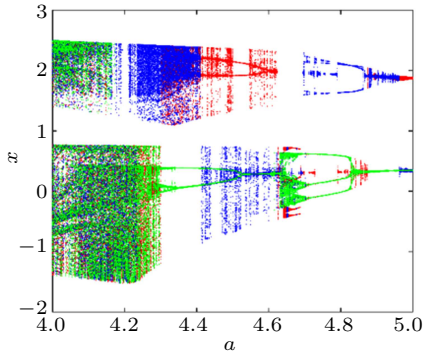


Fig. 5. Bifurcation diagrams for different initial values, where green, blue and red orbits corresponding to $(1,1,1,1)$, $(1,-1,1,1)$, $(-0.1,-0.1,0,0)$, respectively.

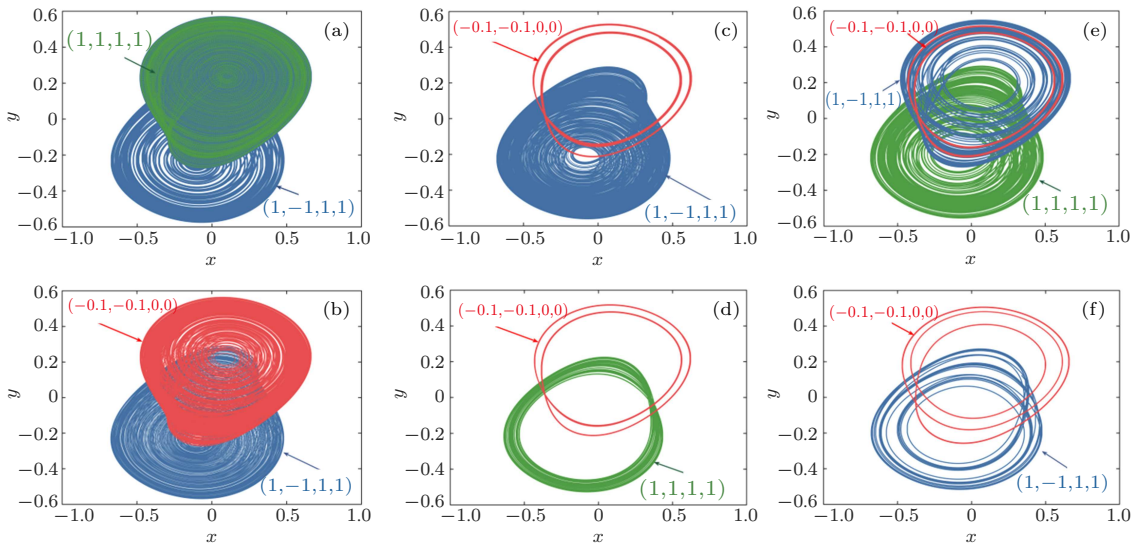


Fig. 6. Coexisting attractor varying with parameter a, where (a) $a = 4.24$, (b) $a = 4.26$, (c) $a = 4.35$, (d) $a = 4.42$, (e) $a = 4.48$, (f) $a = 4.76$.

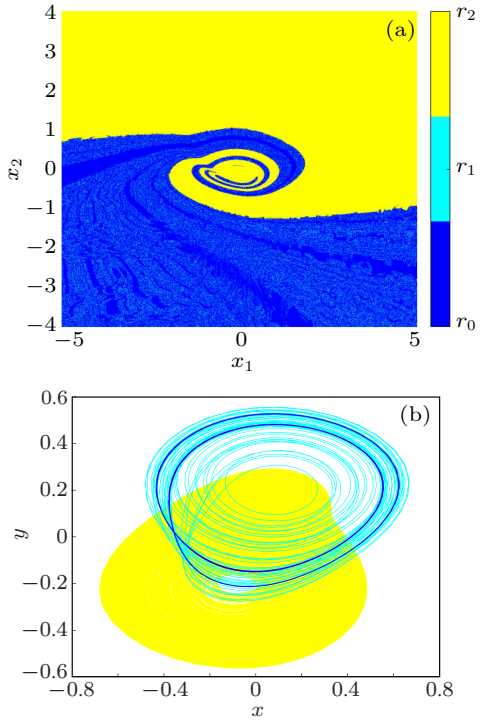


Fig. 7. (a) Attraction basin for multi-attractor coexistence with parameters $a = 4.35$, $b = 0.1$, $c = 1$. (b) Phase diagram orbits in the x and y planes for different initial conditions.

depicted by a green dashed line. As shown in Fig. 6(b), when $a = 4.26$, two single scroll attractors with different scroll directions are observed. As shown in Fig. 6(c), when $a = 4.35$, the chaotic state disappears and turns into a periodic state with the initial value $(-0.1, -0.1, 0, 0)$, but with the initial value condition $(1, -1, 1, 1)$, the system keeps chaotic and still has a single scroll attractor. As shown in Fig. 6(d), when parameter a increases to 4.42, the coexistence of quasi-periodic and periodic attractors can be observed under the initial values $(1, 1, 1, 1)$ and $(-0.1, -0.1, 0, 0)$. As shown in Fig. 6(e), when $a = 4.48$, three kinds of different behaviors, namely, single scroll, periodic and quasi-periodic attractors, can be observed. As shown in Fig. 6(f), when $a = 4.76$, the coexistence of three periods and quasi-periodic attractors can be observed.

The basin of attraction of a chaotic system is the set of points where the motion trajectories converge to the corresponding attractors under the determined system parameters and different initial conditions. When the system parameters are determined as $a = 4.35$, $b = 0.1$ and $c = 1$, the attractor basins and the corresponding phase diagrams for the coexistence of multiple attractors are shown in Figs. 7(a) and 7(b), respectively. The attractor basins are plotted in the x–y plane, and the results show that different attractors can be produced at different initial values, indicating that the dynamical behavior of this network strongly depends on the initial values. The yellow and light blue regions represent chaotic behavior and the dark blue regions represent periodic behavior, respectively.

The phase diagram of the system is drawn according to Fig. 7(a). From Fig. 7(b), the phase diagram orbits are plotted in the x and y planes for different initial conditions, and it can be seen that the system generates chaotic attractors when $z(0) = w(0) = 1$; when $x(0) = 3$, $y(0) = 1$; when $x(0) = 3$, $y(0) = -3.35$; when $x(0) = -4.5$, $y(0) = 0$; and when $x(0) = 4.5$, $y(0) = 0$, the system generates periodic attractor.

4. Multiple scroll attractors in HNN

Using bipolar pulse current or multilevel logic pulse current to stimulate the memristor can make the dynamic behavior of the HNN more complicated.[34] "MLP" represents the multi-level-logic pulse function I_{MLP}, which can be described as

$$I_{\mathrm{MLP}} = \sum_{1}^{n} a_n \mathrm{sign}(\sin(\omega_n t)), \tag{9}$$

where a_n stands for the amplitude of the pulse signal and ω_n stands for frequency. In this section, a multilevel logic pulse

current $I_{\rm MLP}$ is chosen to stimulate the memristor HNN, and after stimulation, the system model of HNN can be described as

$$\begin{cases} \dot{x} = -x + 1.1\tanh(x) + W\tanh(y) + 1.1\tanh(z), \\ \dot{y} = -y - 1.2\tanh(x) + \tanh(y) - 0.14\tanh(z), \\ \dot{z} = -z + 4\tanh(x) - 1.67\tanh(y) + 1.7\tanh(z), \\ \dot{w} = -w + 1.3\tanh(x) + I_{\rm MLP}, \end{cases} \tag{10}$$

and the topology of new HNN is shown in Fig. 8.

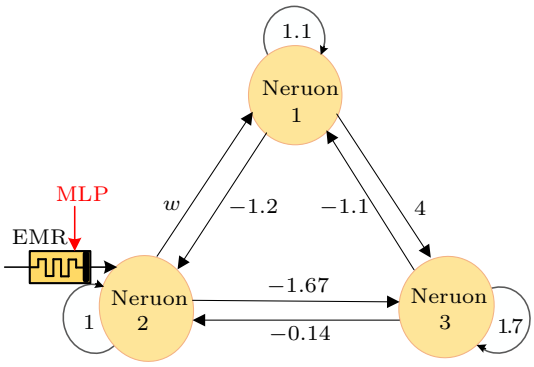


Fig. 8. HNN connection topology after introducing logical pulse.

Due to the introduction of $I_{\rm MLP}$, the original memristor model is changed, which can be described as

$$\begin{cases} i = W(v_0)v = [a - b\tanh(v_0)]v, \\ \dot{v}_0 = -v_0 - v + I_{\rm MLP}, \\ W(v_0) = a - b\tanh(v_0), \\ I_{\rm MLP} = \sum_{1}^{n} a_n \text{sign}(\sin(\omega_n t)). \end{cases} \tag{11}$$

Without loss of generality, the internal parameters of the memristor are set to $a = 3.6$, $b = 0.1$ and parameter n of $I_{\rm MLP}$ is set to 2. The amplitude and frequency of the pulse signal are respectively set to $a_1 = 0.21$, $\omega_1 = 0.024$, $a_2 = 0.43$, $\omega_2 = 0.016$, $a_3 = 0.85$ and $\omega_3 = 0.032$. Sinusoidal excitation voltages $v = v_i \sin(2\pi f t)$ are applied to the memristor with different frequencies, where v_i is the voltage amplitude and f is the voltage frequency. When the frequency f and voltage amplitude v_i take different values, the voltage–current characteristics of a pulse-controlled memristor are shown in Fig. 9. The pulse controlled memristor is a tight pinched hysteresis loop on the v–i plane, which is constricted at the origin. It can be seen that the area enclosed by the curve decreases with frequency increasing and tends to be a single value function. But with amplitude increasing, the area increases gradually. This conclusion proves that the pulse-controlled memristor proposed in this paper belongs to the category of generalized memristor.

As shown in Fig. 10, when different pulses are applied to the memristor, the system can generate different numbers of scroll attractors. When no pulse stimulation is applied to the memristor, the original system can generate a double scroll attractor. The phase diagram of the w–z plane is shown in Fig. 10(a). When $n = 1$, $a_1 = 0.21$, $\omega_1 = 0.024$, the system can generate four scroll attractors, and the phase diagram of the w–z plane is shown in Fig. 10(b). When $n = 2$, $a_2 = 0.43$, $\omega_2 = 0.016$, the system can generate eight scroll attractors, and the phase diagram of the w–z plane is shown in Fig. 10(c). When $n = 3$, $a_3 = 0.85$ and $\omega_3 = 0.032$, the system can generate sixteen scroll attractors, and the phase diagram of the w–z plane

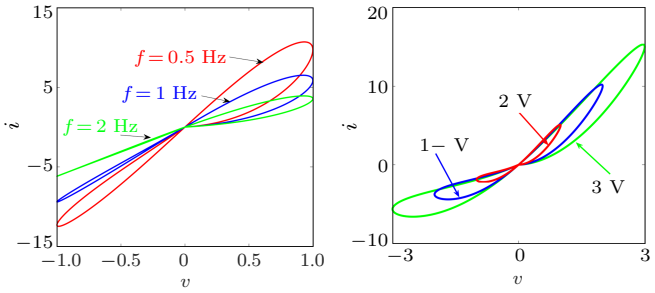


Fig. 9. Tight pinched hysteresis loop characteristics of the pulse controlled memristor.

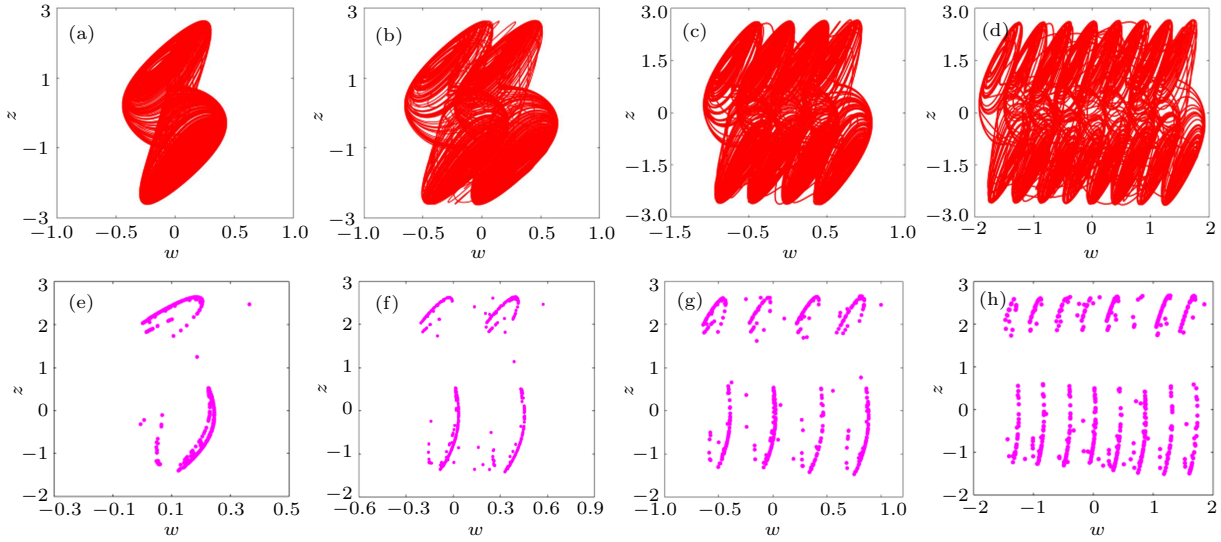


Fig. 10. Multi-double scrolls phase diagram and Poincare cross section diagram under different pulse stimulation, (a) and (e) $n = 0$; (b) and (f) $n = 1$; (c) and (g) $n = 2$; (d) and (h) $n = 3$.

is shown in Fig. 10(d). The Poincare section diagram corresponding to the above scroll attractors is shown in Figs. 10(e)–10(f). It is obvious that the continuous curve of the upper and lower distribution confirms the generation of the chaotic attractors of the multi-double scrolls.

From the phase diagram, it can be seen that when n pulse signals stimulate the memristor, the system can generate 2^{n+1} scroll attractors in the w–z plane, that is to say, the system can control the number of scrolls.

When the system is stimulated by a logical pulse, the unstable saddle focus of indicator 1 and the unstable saddle focus of indicator 2 in the system will increase in pairs. One unstable index 2 saddle focus corresponds to the generation of a scroll attractor, while the index 1 saddle focus is used as a bond track to connect the two scrolls and finally generate a double scroll attractor. In Fig. 11, the equilibrium points E_1 to E_{16} correspond to the unstable index 2 saddle focus, generating a single scroll attractor. The equilibrium point E_{17} to E_{24} corresponds to the unstable index 1 saddle focus, which generates a bond track and connects two single scrolls to become a double scrolls attractor.

In order to verify the higher complexity of the HNN system under impulse stimulation, this paper carries out a spectral entropy complexity comparative analysis experiment: the complexity of the sequence is evaluated by the spectral entropy (SE) value, which examines the frequency distribution characteristics of the sequence in the transform domain. The higher value of spectral entropy can reflect that the original signal has higher randomness, implying that the sequence has stronger randomness. In this study, the parameter a is chosen as an analytical object to explore the complexity of chaotic sequences. When the value of parameter a is in the range of (3, 5), the spectral entropy distribution is shown in Fig. 12(a), at which the average SE value is 0.444. According to Refs. [35–37], when the parameters b, c and d are in the ranges of (0, 1), (0.2, 1.8), (0.2, 1.8), and (0, 1.4), respectively, the corresponding spectral entropy distributions are plotted as shown in Figs. 12(b)–12(d), and the respective average SE values are 0.339, 0.204 and 0.206, respectively. From the simulation results, system (4) exhibits higher SE complexity compared to the other systems, and therefore, the chaotic sequences generated by the multiple scroll chaotic system have a stronger randomness, which can provide higher security when applied to encrypted communication and other fields.

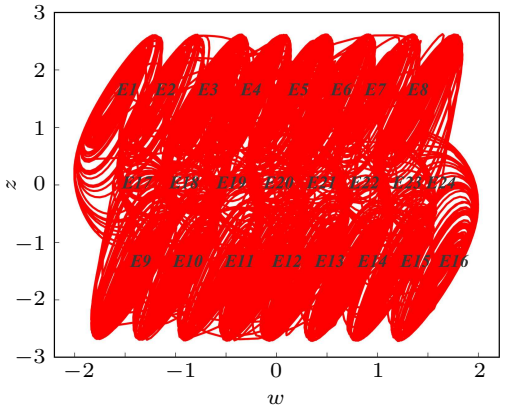


Fig. 11. The equilibrium point of the multi-double scrolls phase diagram when $n = 3$.

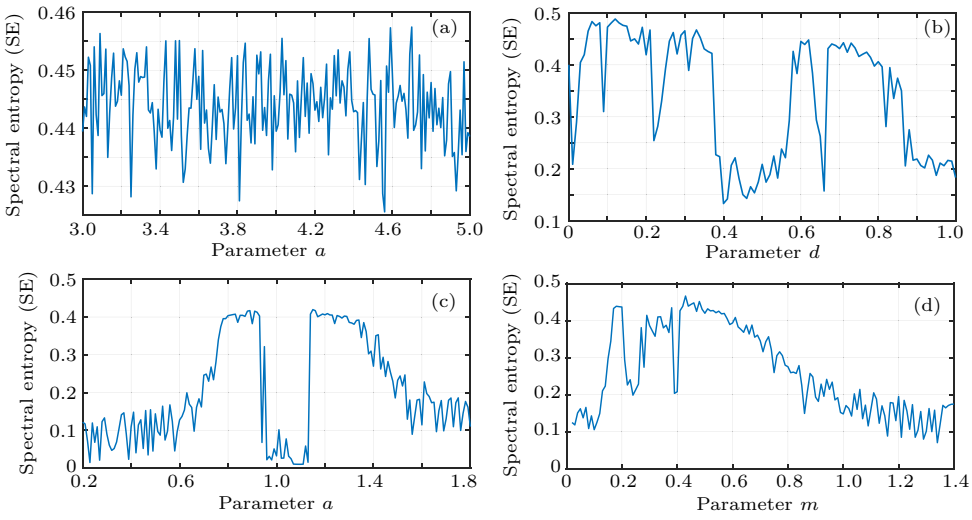


Fig. 12. Comparative analysis of spectral entropy.

5. The circuit of memristor HNN

Before implementing the neural circuit, it is necessary to introduce the multilevel logic pulse function circuit, the hyperbolic tangent function circuit, and the hyperbolic-type memristor circuit. As shown in Fig. 13, when the voltage is input, the current can be calculated as $I_{\mathrm{MLP}} = \sum_1^n \frac{\mathrm{sign}(\sin(2\pi F_{an} t))}{R_{an}}$, where $R_{\mathrm{s}} = 13.5\ \mathrm{k\Omega}$, $R_{\mathrm{k}} = 1\ \mathrm{k\Omega}$, and switch S can control the number of logical pulse functions in the access circuit.

In a hyperbolic tangent function circuit, the input and output relations can be expressed as $W(v_0) = a - b\tanh(v_0)$,

where $R_{\rm F} = 520\ \Omega$, $R_{\rm C} = 1\ {\rm k}\Omega$, $I_0 = 1.2$ mA.

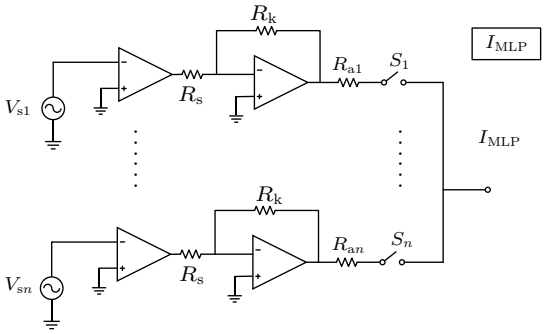


Fig. 13. Multilevel logic pulse function circuit.

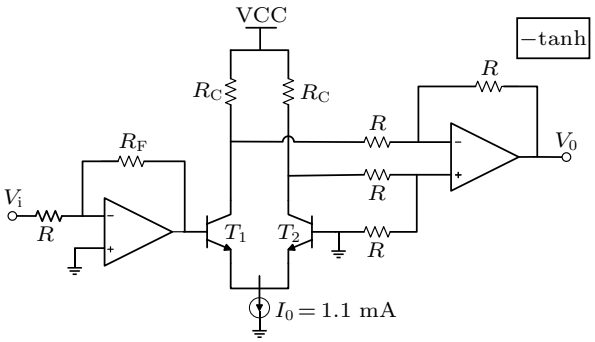


Fig. 14. Hyperbolic tangent function circuit.

The hyperbolic-type memristor circuit is shown in Fig. 15. Its nonlinear conductance function can be expressed as $W(v_0) = a - b\tanh(v_0)$.

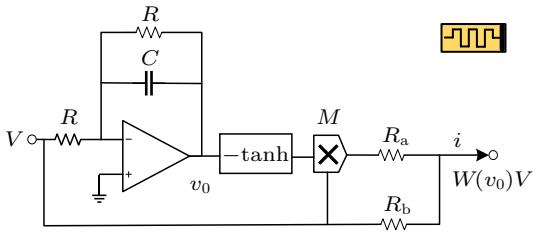


Fig. 15. hyperbolic-type memristor circuit.

The HNN circuit diagram under pulse-controlled memristor stimulation is shown in Fig. 16. When all switches S are disconnected, only the original hyperbolic-type memristor is introduced into the system. When the switch S is closed, the system is stimulated by pulse.

According to Kirchhoff's law, the circuit state equation can be obtained as

$$\begin{aligned} RC\frac{{\rm d}v_1}{{\rm d}t} &= -v_1 + \frac{R}{R_1}\tanh(v_1) + \left(\frac{R}{R_{\rm a}} - \frac{R}{R_{\rm b}}\tanh(v_0)\right)\tanh(v_2) \\ &\quad + \frac{R}{R_2}\tanh(v_3), \\ RC\frac{{\rm d}v_2}{{\rm d}t} &= -v_2 + \frac{R}{R_3}\tanh(v_1) + \frac{R}{R_4}\tanh(v_2) - \frac{R}{R_5}\tanh(v_3), \\ RC\frac{{\rm d}v_3}{{\rm d}t} &= -v_3 + \frac{R}{R_6}\tanh(v_1) + \frac{R}{R_7}\tanh(v_2) - \frac{R}{R_8}\tanh(v_3), \end{aligned}$$

$$RC\frac{{\rm d}v_4}{{\rm d}t} = -v_4 + \tanh(v_1) + I_{\rm MLP}, \tag{12}$$

where RC is the integral time constant, v_1, v_2, v_3 and v_4 are the voltages of the four integrated circuit capacitors, respectively, $v_{\rm a}$, $v_{\rm b}$ and $v_{\rm c}$ can be obtained through the inverter circuit. Let $RC = 10\ \mu$s, where $R = 10\ {\rm k}\Omega$ and $C = 1$ nF. According to the system parameters and Kirchhoff's law, the remaining circuit parameters can be calculated as $R_1 = 8.69\ {\rm k}\Omega$, $R_2 = 9.09\ {\rm k}\Omega$, $R_{\rm a} = 10\ {\rm k}\Omega$.

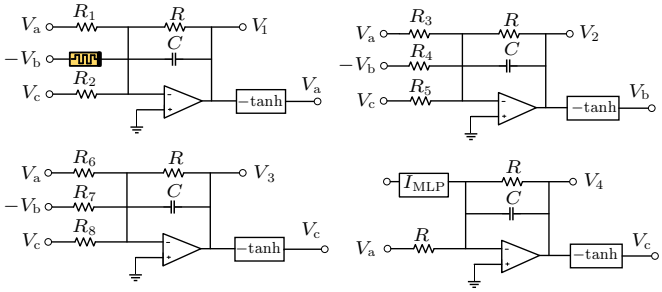


Fig. 16. HNN circuit diagram under pulse-controlled memristor stimulation.

By verifying on the circuit simulation software Multisim 14.0, the actual phase diagram is shown in Fig. 17, which agrees with the theoretical phase diagram mentioned above. Therefore, the existence of an attractor in this chaotic system is verified.

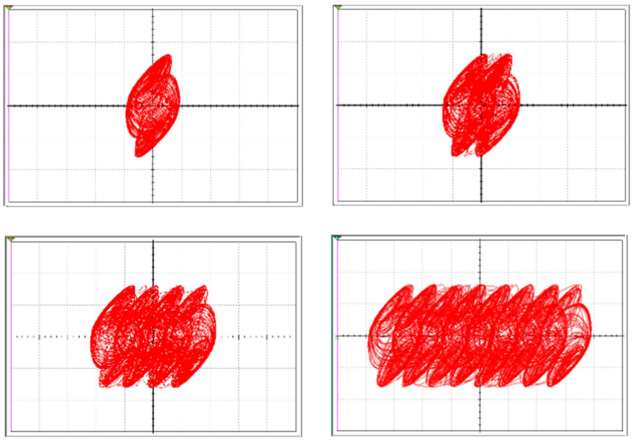


Fig. 17. The w–z circuit simulation diagram with different parameters n.

6. Conclusion

In this paper, we analyze the influence of hyperbolic-type memristors on the dynamic behaviors of HNN. The experimental results show that when the memristor is added to the HNN, the system can generate single scroll, multi-scrolls and periodic attractors. With the change of the internal parameters of the memristor, these attractors can switch back and forth. In addition, small changes in the initial value conditions of the system can induce great changes in the dynamic behavior of the system and lead to the observation of different types of coexisting attractors. Then, on the basis of the original memristor, the number of saddle focus balance points increased from

3 to 6, 12 and 24 by adding pulse stimulation, and the multi-double scrolls attractors of 2, 4 and 8 pairs were generated. Finally, the numerical simulation results are verified by the circuit simulation test. Compared with other memristor HNN models, this memristor HNN model has abundant dynamic characteristics and complex attractors, which has higher application value in the fields of information encryption, chaotic bioengineering, chaotic neural network information processing, and other fields.

However, simulating and analyzing the behavior of multiple double-vortex attractors in high-dimensional memristor neural networks require a lot of computational resources. Complex calculations and analysis can lead to latency problems in real-time applications and limit its practical application in large-scale neural networks. The memristor has the potential to realize complex nonlinear behavior, and although circuit simulations of the proposed system have been performed in this paper, there are still many challenges to implementing multi-double-vortex attractors in actual hardware, such as device consistency, manufacturing process complexity, and performance degradation due to device aging.

Acknowledgements

This paper was supported by the Guizhou Province Natural Science Foundation (Qiankehe Fundamentals–ZK[2023]General-055) and Guizhou Province Science and Technology Support Plan Project (Qiankehe Fundamentals [2023] General-465).

References

[1] Vahid K, Fereidoun R N and Ali S 2022 *Biomedical Signal Processing and Control* **78** 103852
[2] Wang H, Lu Q and Wang Q 2008 *Communications in Nonlinear Science and Numerical Simulation* **13** 1668
[3] Zhou Z W and Wang S 2022 *Physica Scripta* **97** 025206
[4] Ichinose N 2021 *International Journal of Bifurcation and Chaos* **31** 2130003
[5] Yu F, Chen H and Kong X 2024 *Euro. Phys. J. Plus* **137** 434
[6] Yu F, Wu C, Lin Y, *et al.* 2024 *Nonlinear Dyn.* **112** 12393
[7] Lai Q, Lai C, Kamdem D P K, Li C and He S 2022 *International Journal of Bifurcation and Chaos* **32** 2250042
[8] Yang F and Wang X 2021 *Physica Scripta* **96** 035218
[9] Castellanos-Jaramillo J, Castellanos-Moreno A and Corella-Madueño A 2020 *Physica Scripta* **95** 075002
[10] Fang T, Zhang J, Huang S, Xu F, Wang M and Yang H 2019 *Nonlinear Dyn.* **98** 1267
[11] Chen C, Bao H, Chen M, Xu Q and Bao B 2019 *AEU-International Journal of Electronics and Communication.* **111** 152894
[12] Yu F, Kong X, Yao W, *et al.* 2024 *Chaos, Solitons & Fractals* **179** 114440
[13] Chen C, Min F, Zhang Y and Bao B 2021 *Nonlinear Dyn.* **106** 2559
[14] Bao B, Qian H and Xu Q 2017 *Frontiers in Computational Neuroscience* **11** 81
[15] Lai Q and Chen Z 2023 *Chaos, Solitons & Fractals* **170** 113341
[16] Lin H, Wang C, Hong Q and Sun Y 2020 *IEEE Transactions on Circuits and Systems II: Express Briefs* **67** 3472
[17] Bao H, Hu A, Liu W 2019 *International Journal of Bifurcation and Chaos* **29** 1950006
[18] Ge M, Jia Y, Xu Y and Yang L 2018 *Nonlinear Dyn.* **91** 515
[19] Ma M, Xie X, Yang Y, Li Z and Sun Y 2023 *Chin. Phys. B* **32** 058701
[20] Li J, Liu S, Liu W, Yu Y and Wu Y 2016 *Nonlinear Dyn.* **83** 801
[21] Wachtel H, Seaman R and Joines W 1975 *Annals of the New York Academy of Sciences* **247** 46
[22] Giannì M, Liberti M and Apollonio F 2006 *Biol. Cybern.* **94** 118
[23] Haan W D, Flier W M V D, Koene T, Smits L L, Scheltens P and C J 2012 *NeuroImage* **59** 3085
[24] Lin H, Wang C, Yao W and Tan Y 2020 *Communications in Nonlinear Science and Numerical Simulation.* **90** 105390
[25] Zhang S, Zheng J H and Wang X 2021 *Chaos* **31** 011101
[26] Rech P C 2011 *Neurocomputing* **74** 3361
[27] Chen P, Chen Z and Wu W 2010 *Chin. Phys. B* **19** 040509
[28] Han S, Kommuri S, Kwon O and Lee S 2022 *Applied Mathematics and Computation* **423** 126994
[29] Pham V T, Jafari S, Vaidyanathan S, Volos C and Wang X 2016 *Science China Technological Sciences* **59** 358
[30] Zheng P, Tang W and Zhang J 2010 *Neurocomputing (Amsterdam)* **73** 2280
[31] Yu F, Kong X X, Mokbel A A M, Yao W and Cai S 2023 *IEEE Transactions on Circuits and Systems II: Express Briefs* **70** 326
[32] Qin M and Lai Q 2024 *Applied Mathematical Modelling* **125** 125
[33] Wu F, Kang T, Shao Y and Wang Q 2023 *Chaos, Solitons & Fractals* **172** 113569
[34] Etémé A, Tabi C and Mohamadou 2019 *Applied Mathematical Modelling* **125** 432
[35] Sun J, Li C, Wang Z, *et al.* 2024 *IEEE Transactions on Industrial Informatics* **20** 3778
[36] Bao H, Chen Z G, Cai J M, *et al.* 2022 *Science China Technological Sciences* **65** 2582
[37] Lin H, Wang C, Cui L, *et al.* 2022 *Nonlinear Dyn.* **110** 841